Efficient and Adversarially Robust Object Detection

Anton Liu
Dept. of Computer Science, Western University
aliu467@uwo.ca
Supervisor: Professor Roberto Solis-Oba

Abstract

The abstract goes here.

I. Introduction

Object detection, one of the fundamental tasks in computer vision, is used in numerous real-world applications by enabling machines to identify and locate objects within images or videos. Object detection algorithms aim to address two challenges in recognizing objects of interest within complex scenes: where (identifying their spatial extent with bounding boxes) an object is and what (assigning corresponding class labels) an object is. Having this capability is crucial for a wide range of tasks, including pedestrian detection for autonomous driving, object tracking in video surveillance, and product recognition for inventory management. Moreover, object detection serves as a foundational building block for higher-level computer vision tasks such as scene understanding, semantic segmentation, and action recognition, facilitating deeper insights and decision-making capabilities in intelligent systems.

The emergence of deep learning revolutionized object detection, leading to significant advancements in accuracy and efficiency. Convolutional Neural Networks (CNNs) have demonstrated remarkable potential and have been the main research direction in recent years [1]. CNNs are a specialized type of deep learning model designed for processing structured grid data, such as images, where spatial hierarchies of patterns are critical. They are structured with multiple layers, each containing convolutional kernels with learnable weights that detect local patterns like edges, textures, and shapes; as data moves through these layers, the network builds increasingly complex representations, enabling accurate recognition and classification.

In safety-critical applications like autonomous driving, the performance of object detection systems can have severe consequences, jeopardizing human safety and privacy. The fatal accident involving an Uber self-driving car in 2018 illustrates the severe consequences that failures in object detection systems can have. While the performance of deep learning-based object detection models has significantly improved, their vulnerability to adversarial attacks poses a significant challenge to their reliability and security [2]. Adversarial attacks involve maliciously crafted perturbations to input data, which can cause deep neural networks to make incorrect predictions or fail to detect objects altogether [3]. To counter the attacks, adversarial defence is a critical area of research focused on enhancing the robustness of deep learning models against adversarial attacks. While deep learning models are typically optimized to maximize performance on clean images, adversarial training aims to increase performance in adversarial scenarios [4]. Despite the importance of adversarial defence techniques, there are a lot less papers compared to adversarial attack [5]. This asymmetry highlights the need for more research efforts dedicated to adversarial defence in object detection, to mitigate the growing threat posed by adversarial attacks and enhance the robustness of deep learning models in practical settings.

Despite their recent success, deep learning methods are computationally intensive during both training and inference due to the need to process large volumes of data through multiple layers. Training requires updating millions of parameters through backpropagation, while inference demands rapid calculations to generate predictions [6]. To handle their Full Self-Driving (FSD) processing, Tesla install high-performance computing platforms capable of 50 trillion operations per second (TOPS) in their vehicles. This custom chip enables complex CNN models to run while maintaining the low latency necessary for safe autonomous driving. Therefore, as the models get larger and more complex, efficiency becomes an increasing concern. Efficiency can be measured in terms of reductions in computational resources, such as memory usage, processing power, and energy consumption.

In this work, the efficiency of an object detection model is measured by the inference time, because it directly reflects the model's performance in real-world applications, particularly those requiring real-time or low-latency processing. Inference time indicates how quickly a trained model can make predictions, which is critical for tasks like autonomous driving, video-based object detection, or any time-sensitive application. A model with short inference time can handle more data in a given time period, improving overall throughput and user experience.

Various methods can be employed to enhance CNN efficiency, such as transfer learning, quantization, weight sharing, and pruning. Pruning is a key technique for improving efficiency and comes in two forms: unstructured pruning and structured pruning. Unstructured pruning removes individual weights that contribute little to the network's performance, leading to sparser weight matrices. While effective in reducing the number of parameters, unstructured pruning can result in irregular memory access patterns, making it hard to optimize on certain hardware. In contrast, structured pruning removes entire filters/kernels, resulting in a more compact architecture. This type of pruning not only reduces the number of parameters but also decreases the computational load, making it more suitable for real-time deployment on hardware like GPUs or mobile devices. Structured pruning maintains the integrity of the network structure, allowing for faster inference times while maintaining accuracy.

While adversarial robustness and efficiency have individually been explored in CNNs, limited research combines these two areas in object detection. This work aims to bridge this gap by adapting adversarial robustness techniques to efficient object detection frameworks.

II. Background

A. Object Detection

Object detection is a computer vision task that involves both the classification and localization of objects within an image or a sequence of images. If a model is given an input image, the objective of object detection is to produce a set of attribute list, where each list is a detected object. Within each object, the model needs to output the following attributes: class of object, confidence score that an object is present, confidence score that the predicted class is correct, and the object's bounding box in the image (typically Xcenter, Ycenter, width, height). The task requires the model to accurately predict both the semantic category and the precise spatial location of each object, addressing challenges such as scale variation, occlusion, and inter-class similarities.

Over the years, numerous approaches have been proposed to address the challenge of object detection, each leveraging different methodologies and architectures [1]. Traditional methods often relied on handcrafted features, such as Histogram of Oriented Gradients (HOG) or Haar-like features, combined with classifiers like Support Vector Machines (SVM) or Random Forests. While effective to some extent, these methods often struggled with complex scenes and suffered from scalability issues [7]. In contrast, convolutional neural networks (CNNs) have demonstrated significant improvements in object detection performance. By learning hierarchical feature representations directly from raw image data, CNN-based approaches eliminate the need for manual feature extraction, enabling them to capture complex patterns in objects, regardless of variations in pose, scale, or occlusion. Furthermore, CNNs can generalize well across diverse datasets, resulting in enhanced robustness and accuracy. These networks have achieved state-of-the-art results in real-time detection, driven by the development of more efficient architectures and advances in computational power, making them the dominant approach in modern object detection tasks.

To train a CNN model for object detection, a large labeled dataset is required, where each image contains annotations about the objects in the image, including class labels and bounding box coordinates. An object detection model is trained by passing input images through a network that extracts features and learns patterns, with the help of techniques like backpropagation and gradient descent to minimize the error between predicted and true labels. During training, the CNN learns to detect objects by adjusting its weights to improve both classification accuracy and localization precision, ultimately producing a model capable of accurately identifying and locating objects in unseen images.

CNN models for object detection generally consist of a feature extraction backbone and a detection head. The backbone, often a pre-trained deep CNN such as ResNet or VGG, extracts high-level features from images, which are then fed into the detection head to perform localization and classification tasks. Some models, like Faster R-CNN, use a region proposal mechanism, while others like SSD (Single Shot Multibox Detector) predict bounding boxes and class labels in a single pass. YOLO (You Only Look Once) models take a unique approach by dividing the image into a grid and predicting bounding boxes and class probabilities simultaneously, making them highly efficient for real-time applications. YOLOv3, in particular, improves upon earlier versions with better detection at multiple scales, making it an excellent model for balancing speed and accuracy in object detection tasks.

Datasets play a pivotal role in advancing the field of object detection by providing annotated images for model training and evaluation. Many openly available datasets exist online, such as Pascal VOC, ImageNet, and Open Images [8]. Among these datasets, the Microsoft Common Objects in Context (MS COCO) dataset stands out as one of the most comprehensive and widely used benchmarks [9]. Its superiority stems from several factors. Firstly, COCO has a diverse range of object categories, encompassing common everyday objects across 80 distinct classes, including people, animals, vehicles, and household items. This diversity ensures that models trained on COCO generalize well to a wide array of real-world scenarios. Secondly, each image in the dataset is annotated with instance-level bounding box coordinates, and class labels for precise training and evaluation of detection algorithms. Additionally, COCO provides a large-scale dataset comprising over 200,000 images split into training, validation, and test sets, facilitating robust model training and unbiased evaluation [9].

In the context of object detection using the COCO dataset, mean Average Precision (mAP) serves as a robust and reliable metric for evaluating the performance of detection models. mAP calculates the precision at various recall levels, averaged over all object classes and potential Intersection over Union (IoU) thresholds, therefore able to comprehensively assess both localization accuracy and classification performance across multiple classes. IoU is used to assess the degree of overlap between bounding boxes, and is calculated as the area of overlap between two bounding boxes divided by the area of their union.

An IoU value closer to 1 indicates a high degree of overlap, while a value closer to 0 indicates little to no overlap. Therfore, mAP as a metric for object detection ensures that the model is evaluated not only on how well it detects objects but also on the accuracy and confidence of those detections.

B. Adversarial attack

Adversarial attacks are techniques used to manipulate machine learning models, especially neural networks, by introducing small, often imperceptible perturbations to inputs that cause the model to make incorrect predictions. These attacks reveal significant vulnerabilities across various applications, ranging from autonomous driving systems, where an adversarial example might mislead an object detection model into misclassifying traffic signs, to facial recognition, where a slight perturbation can trick a system into misidentifying individuals. In critical domains like medical diagnosis, adversarial attacks pose serious risks by potentially altering predictions for diseases or conditions, leading to incorrect diagnoses or treatment decisions. Several methods exist for generating adversarial attacks, each varying in complexity, impact, and effectiveness.

The Fast Gradient Sign Method (FGSM) is a straightforward, single-step attack that adjusts the input in the direction of the gradient of the model's loss function, making it a fast and computationally efficient way to create adversarial examples. However, its simplicity limits its ability to produce high-quality, robust adversarial examples. In contrast, Projected Gradient Descent (PGD) is an iterative and stronger attack method that applies FGSM repeatedly, with a small step size, projecting each step back within a specified perturbation limit. PGD is often regarded as a universal benchmark for adversarial attacks because it creates more robust and challenging adversarial examples. Additionally, the Carlini & Wagner (C&W) attack is a more sophisticated, optimization-based method known for creating highly effective yet subtle perturbations, which are harder to detect by human observers or defense mechanisms.

C. Efficient Adversarial Robustness

Many papers have attempted to tackle the problem of making CNNs robust to adversarial attacks, and many others focus on making CNNs more efficient. However, not many combined these two important topics to develop CNNs that are both efficient and adversarially robust. Vaddadi et al. showcased an efficient CNN model optimized for adversarial robustness, achieving high classification accuracy and effective resistance to adversarial samples. Another work from Wijayanto et al. explored the vulnerability of CNNs, particularly compressed models used in mobile devices, and investigated methods to enhance their robustness without sacrificing accuracy. Ye et al. presented a framework that combines adversarial training with weight pruning to achieve model compression without sacrificing robustness, addressing the challenge of maintaining both properties simultaneously. Furthermore, Gui et al. introduced an Adversarially Trained Model Compression (ATMC) framework, integrating pruning, factorization, and quantization within a unified optimization structure to achieve compact, adversarially robust models without significant accuracy loss.

Sehwag et al. evaluated the robustness of CNNs under both structured and unstructured pruning. The authors provide a formal definition of the pruning procedure, encompassing pre-training, weight pruning, and fine-tuning, which clarifies the methodology's effectiveness in achieving compact networks without compromising performance. Empirical results demonstrate that the proposed method can maintain an average of 93% benign accuracy (percentage of correctly classified non-modified images) and 92.5% empirical robust accuracy (percentage of correctly classified adversarial examples), while achieving a compression ratio of 10×. Their experimental data showed that their proposed method is effective for both pruning methods, but especially for unstructured pruning.

HYDRA is a seminal work aimed towards improving the performance of machine learning models by the same authors. Sehwag et al. developed a pruning method that is aware of the robust training objective. This is achieved by formulating the pruning process as an empirical risk minimization (ERM) problem combined with a robust training objective, which is solved efficiently using Stochastic Gradient Descent (SGD). The authors also introduced importance score-based optimization, with every weight being initialized with an importance value that is proportional to pre-trained network weights. This change has been shown to help with the final performance and speed of SGD convergence over random initialization. Extensive experiments were performed by testing with CIFAR-10, SVHN, and ImageNet datasets, and with four robust training techniques: iterative adversarial training, randomized smoothing, MixTrain, and CROWN-IBP. HYDRA achieves state-of-the-art performance in both benign and robust accuracy, even at high pruning ratios (up to 99%). The method shows significant gains in robust accuracy while also improving benign accuracy compared to previous works.

The HYDRA pipeline can be described in five steps:

1) Pre-train the network: the CNN is trained on a dataset to minimize a specified loss objective, which is the ERM problem integrated with a robust training objective.
2) Initialize scores: a floating point importance score is assigned to each weight, using the scaled initialization technique. Each weights' score depends on the size of their receptive field (region of the input image that influences the activation of that weight), number of input channels, and magnitude of the weight.
3) Minimizing loss: the weights of the CNN are frozen, but the corresponding importance scores are updated as the loss is minimized. If k weights are to be kept in the end, only top k importance weights will be used for predictions. However, all scores are updated in the backpropagation phase by the calculated gradient.
4) Pruning: using the obtained importance scores that are now frozen, the weights that are found to be less important are pruned away. If the desired pruning ratio is x%, a binary pruning mask is created to only keep weights with top (100-x)% score.
5) Fine-tuning: the pruned network has its parameters updated by training again with the dataset and the robust training objective. The pruning process disrupts the learned representations in the network, and fine-tuning helps it to adapt to these structural changes and re-learn important patterns with fewer parameters. This step partially recovers the performance loss incurred during the pruning phase, and outputs the compressed network.

HYDRA was chosen as the foundation of our work, because of the excellent performance and extensive existent documentation. The performance of HYDRA's initialization and pruning algorithm was strong enough to earn second place in the auto-attack robustness benchmark, and HYDRA's paper has been cited over 100 times since its publication.

Current research on methods for obtaining efficient and adversarially robust CNNs often use image classification as a proof of concept. Image classification is a simpler task compared to object detection, which makes classification models less complex and faster to train, test, and evaluate. This is advantageous for prototyping new techniques or testing optimization methods, however it leaves a gap in assessing the effectiveness of these methods on more complex tasks such as object detection. It presents additional challenges with multi-object recognition, localization, and increased model architecture complexity. No current research paper has fully tested these methods on object detection, limiting our understanding of their performance and robustness in real-world applications.

III. Method

A. Adapting HYDRA to object detection

HYDRA was originally developed for the task of image classification, where the primary objective is to recognize and categorize the types of objects present in an image. While this task is fundamental in many applications, there are scenarios where understanding the spatial arrangement of objects within an image is equally important. This need gives rise to the task of object detection, which not only identifies objects but also localizes them by drawing bounding boxes around each detected object.

To adapt the HYDRA algorithms for object detection, the CNN models used in HYDRA were replaced with YOLOv3. Weights for the parameters of the model that are pre-trained on the COCO dataset are used because the original datasets have been transitioned to COCO to include crucial localization information. To modify the pruning pipeline from object classification to object detection with YOLOv3, several critical modifications were implemented to accommodate the object detection framework.

First, the dataloader of HYDRA was restructured to read and process the COCO dataset, which contains bounding box annotations and multiple object classes within a single image, unlike classification where only a single label per image is needed. Each image's annotations were parsed to include coordinates, width, height, and class labels, with data augmentation applied to enhance robustness. The images are then each padded into a square and resized into 416x416 pixels to ensure compatibility with the default input size of YOLOv3.

Next, some output processing was added. Unlike classification, which produces a single prediction per image, YOLOv3 outputs a 2D matrix of bounding boxes, confidence scores, and class probabilities for each grid cell. This output was parsed to filter out low-confidence predictions using a confidence threshold of 0.5, chosen for a balance between filtering out uncertain predictions and retaining potentially accurate ones. After this initial filtering, Non-Max Suppression (NMS) is applied to remove redundant bounding boxes that may overlap significantly for the same object. YOLOv3 often detects multiple bounding boxes around a single object, especially when objects are large or highly prominent. A higher IoU between bounding boxes indicates a higher chance that they are detecting the same object. This post-processing step ensures that the final output contains only the most probable predictions.

Detection outputs are saved in CSV format, and each entry contains the image identifier, predicted bounding box coordinates, confidence score, and predicted class label. From this, mAP performance is calculated using the pycocotools library, an evaluation toolset that provides metrics specifically for object detection. Pycocotools compares the model's predicted bounding boxes against ground truth annotations across multiple IoU thresholds (from 0.5 to 0.95, in increments of 0.05) and averages the precision over these thresholds. This approach captures the model's performance in detecting objects of varying sizes and levels of overlap, providing a robust measure of detection accuracy for YOLOv3 in this adapted setting.

B. PGD attack

The Projected Gradient Descent (PGD) attack, an iterative and robust approach, refines the FGSM method by taking multiple, bounded steps in the direction of the gradient. After each step, the perturbation is projected back to ensure it stays within a specified range of the original input, thus maintaining perceptual similarity. PGD is particularly effective at generating stable adversarial examples that consistently fool models across different test conditions and architectures. Its iterative nature and ability to overcome defenses, such as adversarial training, make PGD a powerful tool for exploring model vulnerabilities. As a result, PGD is often the chosen method for evaluating the robustness of machine learning models, making it the attack method of choice for this work.

Implementing the PGD (Projected Gradient Descent) attack for YOLOv3 object detection involves generating adversarial perturbations that lead the model to misdetect or fail to detect objects. PGD, an iterative attack method, aims to maximize the YOLOv3 model's prediction error by making small, carefully calculated perturbations to the input image. To apply PGD to YOLOv3, we start by calculating the gradient of the loss with respect to the input image. At each iteration, a small step is taken in the direction of this gradient, adding a bounded perturbation to the input image. The step size and the overall perturbation limit (ε) are hyperparameters that control the severity of the attack, with each step projected back to ensure the perturbation stays within this ε-bound. The process repeats for a fixed number of iterations or until the adversarial effect is achieved. Specifically for this work, when each pixel value is from 0 - 1, 5 steps are taken at 0.02 each, with the ε-bound as 0.05. This is a small enough perturbation that is not obvious to the human eye, but strong enough to decrease the model accuracy.

C. Implementing unstructured and structured pruning

In addition to the unstructured pruning techniques utilized in the original HYDRA method, structured pruning was implemented for a comparative analysis between the two approaches. As it can lead to more substantial reductions in model size and computational complexity while preserving the overall architecture of the network. This was inspired by the authors' previous work where they demonstrated the effectiveness of employing both structured and unstructured pruning strategies. This comparison allows for a deeper understanding of the trade-offs associated with each pruning strategy, particularly in terms of model accuracy, robustness, and efficiency.

The structured pruning technique is implemented by focusing on reducing entire kernels, as opposed to individual neurons in unstructured pruning. Specifically, structured pruning evaluates the importance of each kernel in convolutional layers, and makes pruning decisions in the higher kernel level instead of the lower, more granular weight level. The kernel importances are each calculated by averaging the importance of all the weights inside the kernel. This means that with the five-step HYDRA pipeline, changes had to be made in the pruning step where the binary pruning mask is applied at the level of kernels. An additional computation step is added to process the kernels' importance, and ensures that all the weights inside have the same value in the binary mask. The mask is a tensor of the same shape as the network's weights, where each element is either a 0 or a 1. The elements in the mask indicate whether a corresponding weight should be pruned (set to zero) or retained. This is more efficient than setting the model's pruned weights to 0.

D. New initialization technique

The scaled initialization method was developed for HYDRA as a better alternative to random initialization for determining the importance of parameter weights in a CNN. However, there are many different methods that can estimate how much each parameter weight contributes to the final output. DeepLIFT (Deep Learning Important FeaTures) is a method that explains neural network outputs by attributing differences in output to changes in input features relative to a defined reference input (often set as an all-zero input or an input with average values). It calculates contribution scores for each feature by measuring their impact on the output difference from the reference state, using specific rules like the RevealCancel rule to enhance accuracy. The RevealCancel rule is designed to handle situations where positive and negative contributions from inputs interact, potentially canceling each other out in non-linear layers. By separating and calculating the effects of positive and negative components independently, RevealCancel captures dependencies between inputs that might otherwise be overlooked, providing a more accurate attribution of each input's contribution to the output. This approach offers a more efficient and interpretable means of understanding neural network predictions compared to traditional gradient-based methods, providing valuable insights into feature importance and model behaviour. Therefore, DeepLIFT was used to initialize the weights' importance in this work.

The DeepLIFT implementation leverages the Captum library, a model interpretability and understanding library for PyTorch. Captum supports a variety of attribution methods, including DeepLIFT, which simplifies the integration of interpretability techniques into deep learning models. Here, DeepLIFT is used to replace steps 2 and 3 in the original HYDRA pipeline by calculating importance scores instead of minimizing a loss function directly. With DeepLIFT, each weight in the network is assigned an attribution score, a measure of how much it contributes to the model's final output, relative to a baseline or reference input. This approach bypasses the limitations commonly associated with gradient-based methods, such as vanishing gradients in saturated activation functions (like sigmoid or tanh) and the appearance of thresholding artifacts. In gradient-based methods, the gradient can become zero in regions where the network's output saturates, making it difficult to identify important features or connections.The DeepLIFT scores are then used directly to generate a binary mask that determines which weights, filters, or kernels should be pruned, targeting those with minimal contribution to the network's output. This process eliminates the need for traditional weight initialization and iterative loss-based minimization during pruning, as the pruning decision is made based on clear, interpretable scores that indicate each weight's significance.

IV. Experiments

Five different scenarios are experimented with. The first four are all with normal COCO images: unstructured pruning with DeepLIFT initialization, unstructured pruning with HYDRA initialization, structured pruning with DeepLIFT initialization, structured pruning with HYDRA initialization. This lets us compare the performance differences between the initialization methods, as well as the different pruning strategies. The last one is structured pruning with DeepLIFT initialization with the same COCO images turned to greyscale, which lets us compare the performance of the method between colored and greyscale images.

Within each scenarios, 10 experiment runs are conducted at each of the 9 chosen pruning ratios: 0%, 25%, 50%, 65%, 75%, 85%, 90%, 95%, 99%. These ratios give enough granularity to prevent gaps in data. In each run, the HYDRA pipeline is followed. The pre-trained YOLOv3 model is first trained for adversarial robustness, and the importance scores are initialized (with either DeepLIFT or scaled initialization). Then, the model with its importance scores are used for all 9 pruning ratios, creating 9 differently pruned models. Each of these models are evaluted with pycocotools to get the resulting mAP performance, with the inference time per image also measured. This process is repeated for all 10 runs per scenario, generating 5 x 9 x 10 = 450 models. All mAP and inference time results are shown in Appendix A.

One-way ANOVA (Analysis of Variance) tests are used to compare the means of the results to see if they are statistically significantly different. The p-value in ANOVA is a probability that indicates how likely it is to observe the data if the null hypothesis (that all group means are equal) is true. The p-value threshold is set at 0.05 for this work, meaning there is a 5% chance that the results could occur due to random variation if the null hypothesis were correct. If the p-value is less than 0.05, the null hypothesis is rejected, concluding that there is a statistically significant difference between the group means.

A random subset of 50,000 images from COCO dataset is used for the pruning pipeline to reduce training time, and the other 150,000+ images are used as testing to evaluate the performance of the pruned model. Each experiment run elapses approximately 8 hours for pruning, and 40 minutes for inference on the models. All experiments are conducted on a NVIDIA 2070 super GPU.

A. *Initial Observations*

To compare the two importance score initialization methods, the mAP performance of the four different pruning scenarios using normal colored COCO images are plotted in Fig. 1a. Each curve represents a different scenario and connects the average mAP of different pruning ratios. The mAP averages are calculated by taking the mean of 10 independent experiment runs conducted for each pruning ratio in the different scenarios, and are plotted as dots in the same figure. The standard deviations of each of the 10 runs are represented as well, in the form of error bars. The variability in results observed when running the pruning algorithm can be attributed to inherent randomness within the model training and pruning processes. SGD updates the model and importance scores using random selection of mini-batches of images, which will lead to different outcomes in the model's structure and pruning results.

It is obvious from Fig. 1a that the mAP performance of the pruned models decrease as pruning rate increases, because higher pruning rates remove a larger number of parameters from the model, effectively reducing its capacity to learn and retain critical information needed for accurate detection. At lower pruning rates, the model can often maintain a reasonable balance, keeping enough essential weights and filters to perform well. However, as the pruning rate increases, this balance shifts, and the model loses more connections, leading to degraded feature extraction and weaker representations. This degradation particularly impacts the model's ability to detect smaller or overlapping objects, as well as its robustness to variations in object scale, position, and appearance. Thus, with fewer resources to capture these details, the model's accuracy in both localization and classification decreases, resulting in a lower mAP as the pruning rate rises.

In the HYDRA paper, the authors focused more on the models' pruned performance at pruning rates of 90%, 95%, and 99%. However, in adapting the HYDRA pruning method from image classification to object detection, the performance drop at higher pruning rates (beyond 60%) is more pronounced because object detection is inherently a more complex task. Specifically, the higher pruning rates severely limit the model's capacity to retain the fine-grained spatial and contextual information needed to accurately detect and localize multiple objects within an image. This sensitivity to pruning stems from the fact that object detection models rely on detailed feature extraction to differentiate and locate objects across varied scales and positions, a demand that image classification models do not face to the same extent.

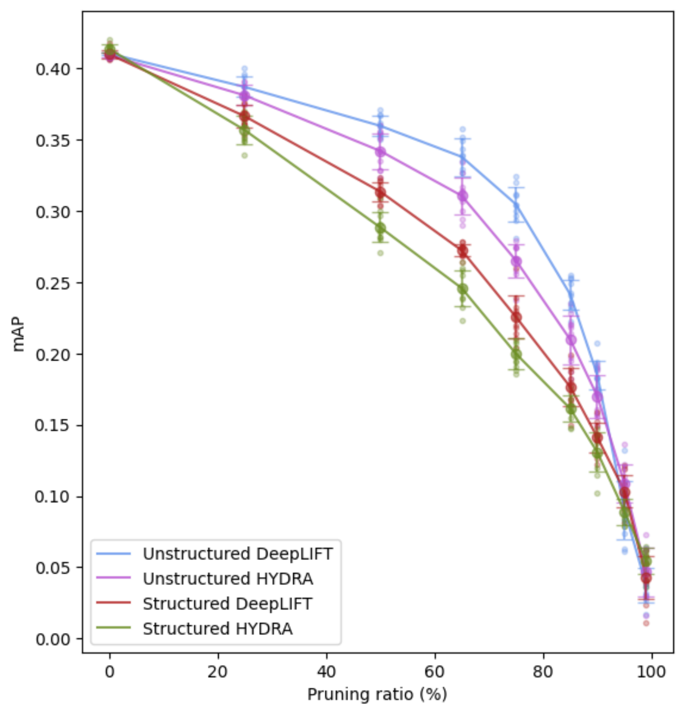

(a) mAP

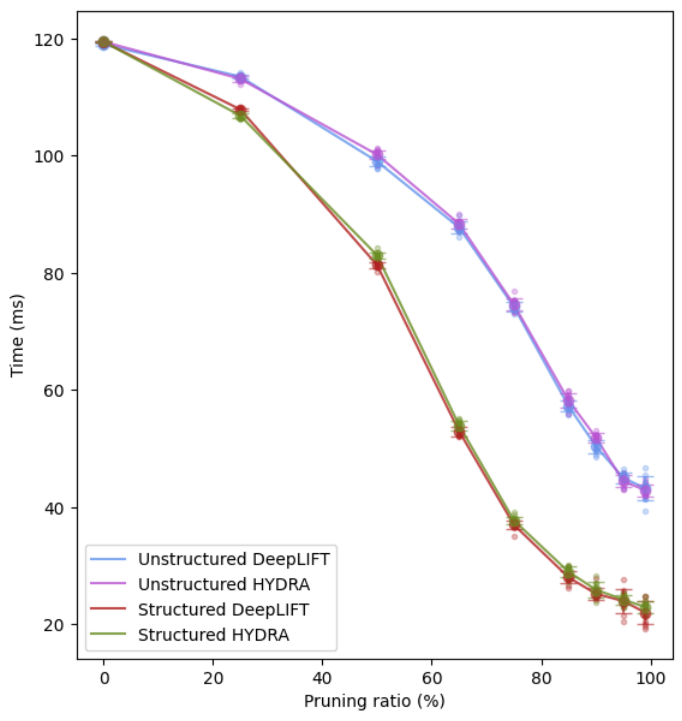

(b) Inference time

Fig. 1: Comparison of proposed approach versus HYDRA with both unstructured and structured pruning, through different pruning ratios

TABLE I: p-values from ANOVA tests on mAP

Pruning ratio	0%	25%	50%	65%	75%	85%	90%	95%	99%
DeepLIFT vs. HYDRA (Unstructured)	1.03e-01	9.53e-02	1.71e-03	3.60e-04	1.57e-06	1.64e-04	2.43e-02	3.54e-02	1.86e-01
DeepLIFT vs. HYDRA (Structured)	1.48e-02	3.60e-02	1.18e-05	1.24e-05	6.91e-04	1.17e-02	8.99e-02	8.87e-03	5.80e-02
Unstructured vs. Structured (DeepLIFT)	6.52e-01	2.35e-05	3.70e-11	4.25e-11	4.20e-10	1.13e-09	5.46e-08	1.09e-01	3.99e-01
Unstructured vs. Structured (HYDRA)	9.00e-04	1.11e-05	1.17e-08	3.05e-09	4.44e-10	6.27e-07	1.80e-05	1.83e-03	2.42e-01

TABLE II: p-values from ANOVA tests on inference time

Pruning ratio	0%	25%	50%	65%	75%	85%	90%	95%	99%
DeepLIFT vs. HYDRA (Unstructured)	1.28e-05	5.61e-02	7.16e-03	1.44e-01	3.96e-01	7.69e-02	4.37e-03	2.05e-01	6.64e-01
DeepLIFT vs. HYDRA (Structured)	5.13e-01	1.81e-06	2.80e-06	1.37e-02	4.21e-02	6.36e-02	2.06e-01	7.33e-01	2.15e-01
Unstructured vs. Structured (DeepLIFT)	1.75e-04	4.13e-19	4.31e-21	1.07e-24	2.76e-26	2.02e-22	6.17e-21	1.85e-16	1.68e-14
Unstructured vs. Structured (HYDRA)	8.70e-01	2.76e-17	1.03e-21	8.97e-26	3.45e-25	1.30e-21	3.55e-21	2.36e-20	1.56e-19

B. *DeepLIFT vs Scaled initialization*

When comparing the mAP performance between models pruned using DeepLIFT initialization and scaled initialization, the former performs better in the 50%-85% pruning ratio range for both pruning methods. The one-way ANOVA tests confirm the conclusion with all p-values in the range under the 0.05 threshold, as shown in Table I. Using DeepLIFT to set importance scores for pruning can be more effective than scaled initialization because DeepLIFT directly calculates the contribution of each weight or neuron to the final output, rather than relying solely on the magnitude of the weights. In scaled initialization, importance is often inferred from the size or magnitude of weights, assuming larger weights contribute more to the model's performance. However, this approach doesn't account for the complex, non-linear relationships between weights and the model's predictions. Large weights might not always be crucial to the output, especially if they are part of redundant or less influential paths in the network. DeepLIFT, on the other hand, provides an attribution score for each weight by measuring its actual impact on the model's output relative to a reference state. This attribution-based approach is more precise, as it captures how each weight contributes to the final prediction, rather than just its size. By focusing on weights that genuinely affect the model's decisions, DeepLIFT can help retain the most functionally important components of the network during pruning, leading to a more efficient model that maintains higher performance even with fewer parameters. This tailored pruning is particularly valuable in complex tasks like object detection, where specific features and spatial relationships are critical for accurate predictions.

When comparing the inference time between pruned models using the two different initialization methods in Fig. 1b, there is not a clear difference between the methods with both unstructured and structured pruning. Regardless of the initial scoring method, the pruning algorithm aims to reduce the network to a target pruning rate, resulting in a final model whose inference efficiency depends primarily on its size and structure rather than on the specific initial importance scores. The p-values from ANOVA tests in Table II mostly support the observation, with most of them above 0.05. However, DeepLift initialization does show small improvements over scaled initialization at 50% pruning ratio for both pruning methods.

Interestingly, the curve that connects different pruning ratios shows an "S" shape. The curve starts with a gentle decline, followed by a steeper drop in the middle stages, and then a plateau or slower reduction at high pruning rates. In the early stages of pruning, inference time may decrease relatively slowly. This is because removing a few parameters doesn't significantly reduce the computation time or memory usage. As pruning increases, the network becomes smaller, and inference time tends to decrease more significantly, especially when a substantial portion of the network is pruned. Beyond a certain threshold, aggressive pruning can introduce sparsity that makes it harder to compute efficiently. At this stage, the inference time may be mostly from hardware bottlenecks such as memory access.

Lastly, when using the DeepLIFT initialization method over HYDRA's scaled initialization, there is an increase in the time taken to initialize the importance scores. Scaled initialization need on average 18 seconds, however DeepLIFT requires almost triple the time at 49 seconds on average. There may be several reasons why DeepLIFT takes longer to run compared to scaled initialization. First, DeepLIFT's reliance on reference-based computations involves calculating the difference between each neuron's activation and a chosen baseline or reference state, which is a more involved process than simply using the magnitude of the neurons' weights. This difference-from-reference approach allows DeepLIFT to propagate importance scores accurately, even when gradients are zero, but it adds an additional layer of computation. Additionally, DeepLIFT's optional rules, like RevealCancel, require separate treatment of positive and negative contributions at each neuron, which can double the amount of computational effort. This is especially demanding in deep networks with complex interactions, where the RevealCancel rule must carefully handle interdependencies among inputs to ensure correct importance scores.

C. unstructured vs structured

Examining the performance difference between unstructured and structured pruning, Fig. 1a shows that unstructured pruning consistently has higher mAP than structured pruning for both initialization methods, for the pruning ratio between 25%-90%. This is supported by p-values from ANOVA tests in Table I. Structured pruning generally results in lower mAP compared to unstructured pruning because it removes entire filters, channels, or even layers, which directly impacts the model's architecture and reduces its ability to capture fine-grained information. By removing whole structures, such as convolutional filters, structured pruning creates gaps in the model's feature extraction capabilities, leading to a less detailed representation of the input. This is particularly detrimental to object detection tasks that rely on capturing diverse features across multiple scales and locations. As a result, structured pruning often has a more pronounced negative effect on mAP, as the model's capacity to accurately locate and classify objects diminishes.

While the initialization method did not have a significant effect on the inference time performance, Fig. 1b shows a significant difference between the two pruning methods. As the pruning rate increases, there is an increasing gap in the time needed for the pruned models to evaluate an image. Starting from 65% pruning ratio, structured pruned models require only approximately half the time compared to a unstructured pruned model at the same pruning ratio. The one-way ANOVA tests confirm these observations in Table II. Structured pruning excels in improving inference time because it results in a more regularized and optimized network architecture. Unlike unstructured pruning, which removes individual weights sparsely throughout the network, structured pruning produces a model with fewer filters or layers but with a consistent structure that is easier for hardware like GPUs to process. This regularity allows for better memory access patterns and more efficient use of processing resources, leading to faster computations during inference. Consequently, while structured pruning may sacrifice some accuracy in mAP, it provides a significant boost in inference speed, making it a practical choice for applications requiring real-time performance.

D. effect of greyscale on performance

TABLE III: p-values from ANOVA tests on mAP

Pruning ratio	0%	25%	50%	65%	75%	85%	90%	95%	99%
Greyscale vs Colour (Unstructured DeepLIFT)	1.13e-23	1.74e-15	1.06e-13	1.18e-11	2.53e-12	2.77e-10	1.75e-05	9.25e-02	5.06e-01

TABLE IV: p-values from ANOVA tests on inference time

Pruning ratio	0%	25%	50%	65%	75%	85%	90%	95%	99%
Greyscale vs Colour (Unstructured DeepLIFT)	6.11e-09	2.07e-07	1.14e-05	4.42e-04	2.08e-01	5.59e-01	2.62e-01	3.98e-02	4.82e-01

Next, the performance of the pruning pipeline is evaluated with greyscale images. The training images are the same ones used in previous parts, but converted to greyscale using the Rec. 601 Standard. The algorithm uses a weighted average with standardized weights on the red (0.299), green (0.587), and blue (0.114) channels to balance human eye sensitivity. The greyscale image is then duplicated into all three channels so that it conforms to the shape of data accepted by the YOLOv3 model. In this experiment, the unstructured DeepLIFT variation of the pruning pipeline is used, since it yields the best mAP performance.

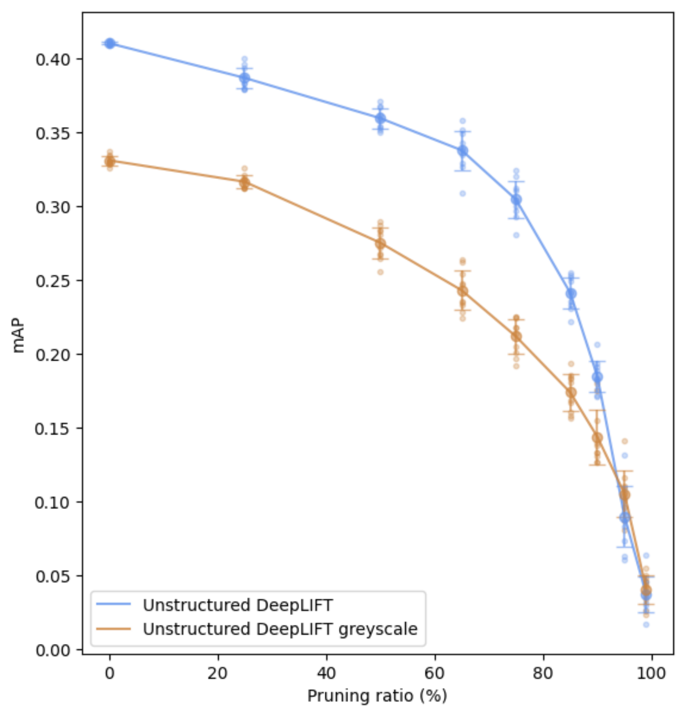

(a) mAP

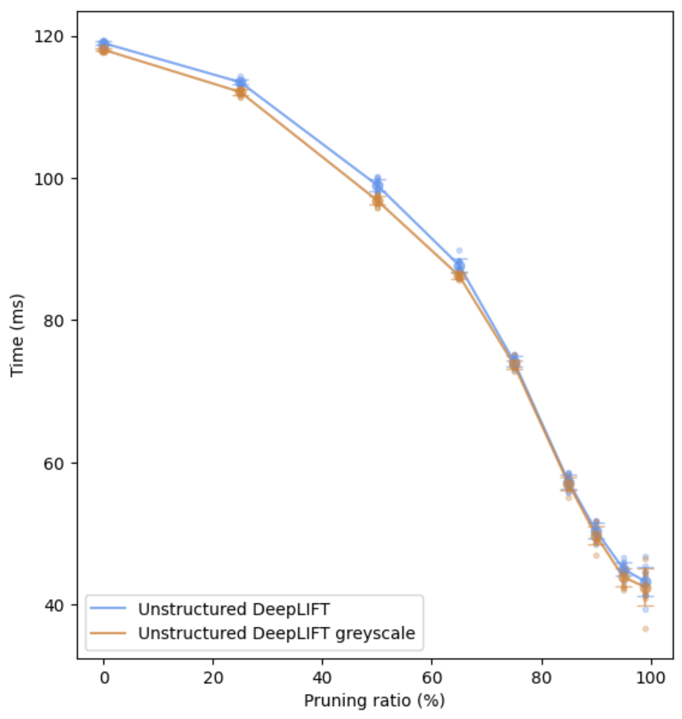

(b) Inference time

Fig. 2: Comparison of performance between color and greyscale images on the proposed method

In the mAP performance shown in Fig. 2a, the models trained with greyscale images perform much worse than one trained with colored images. The discrepency between models are the largest at the lower pruning ratios, from 0% to 65%, and the two models start converging as the pruning ratio increases. At 95% and 99% pruning ratio, the color (or absense of color) has no effect on the model performance. These observations are confirmed with the ANOVA test p-values in Table III.

The observed performance gap between models trained on greyscale versus colored images can be explained by the reduced information available in greyscale images. Object detection models, particularly those like YOLOv3, leverage color information to help distinguish objects from the background and from each other, as well as to capture subtle variations in texture, lighting, and shading that contribute to accurate object localization and classification. In colored images, the model can use the distinct red, green, and blue channels to capture these variations, which aids in creating a more detailed and nuanced feature representation of each object. In contrast, greyscale images provide only intensity information, limiting the model's ability to distinguish certain objects based on color-related features, and this can negatively impact mAP performance, particularly at lower pruning ratios where the network retains more parameters and thus has greater capacity to process detailed information. For example, without color information, it becomes challenging for the model to distinguish between objects like lemons and limes, as both share similar shapes and textures; the absence of yellow or green color cues can lead to confusion in classification.

At lower pruning ratios (0% to 65%), where more network parameters are retained, the color information plays a significant role in enhancing model performance, as the model can make full use of color-based features. The lack of color in greyscale images leads to a noticeable drop in mAP at these pruning rates because the model has fewer cues to differentiate objects and backgrounds, resulting in less precise detection. As the pruning ratio increases, however, the network becomes increasingly constrained, losing

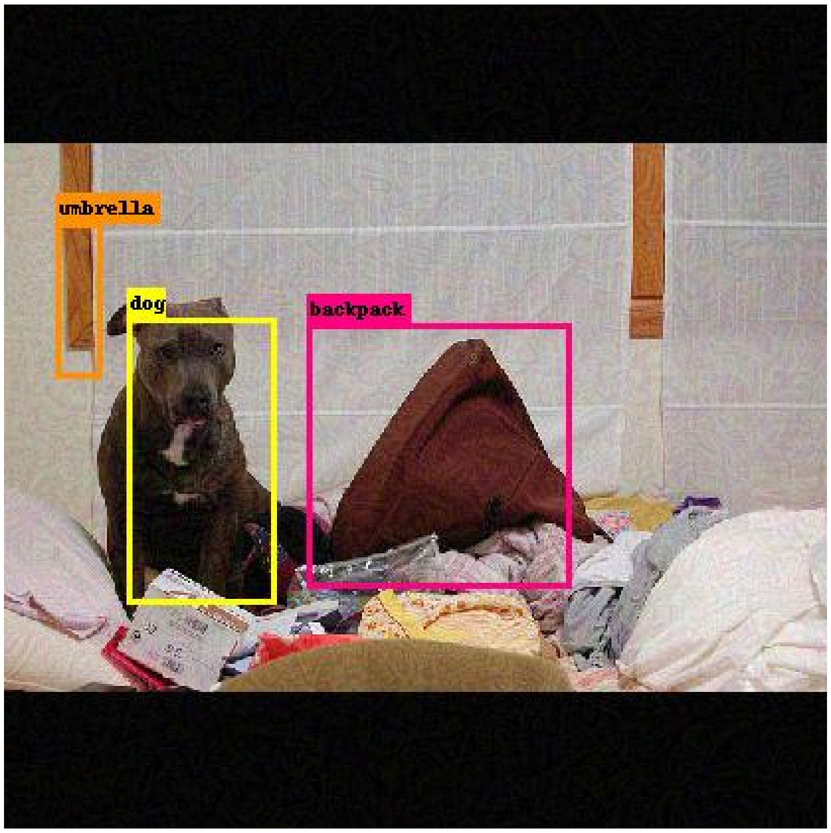

Fig. 3: COCO image 22192 results from models pruned with different initialization, structure, and ratio

a substantial amount of capacity to capture and process intricate features, including those related to color. At higher pruning rates (95% and 99%), both greyscale and color-based models are similarly limited in their feature extraction abilities due to the severe reduction in parameters. This means that even in the color-based model, the remaining network capacity is not sufficient to utilize the color information effectively, leading to a convergence in performance between the greyscale and color models. Essentially, at extreme pruning levels, the model's ability to leverage additional color information diminishes, resulting in similar mAP performance for both greyscale and color inputs.

When considering the inference time performance, it can be observed from Fig. 2b that the greyscale-trained models are slightly faster at evaluting images at smaller pruning ratios until 65% pruning ratio. This slight improvement in inference speed can be attributed to the simpler feature extraction process involved when working with greyscale images. Since greyscale images lack color information, the model processes fewer distinct features per image, requiring less computation to analyze intensity-only patterns compared to the more complex, multi-channel color features. In color images, the model needs to process three channels, each containing unique information that must be integrated to capture subtle differences in texture, color gradients, and object boundaries. As the pruning ratio increases, the network's capacity to process any detailed information—whether from color or greyscale—declines sharply. This reduction in complexity due to aggressive pruning diminishes the initial speed advantage observed with greyscale inputs. By the time the pruning ratio exceeds 65%, both greyscale and color-trained models are similarly limited in their feature extraction abilities, leading to convergence in inference time performance.

E. Sample Images

V. Conclusion

Conclusion here.

Appendix A
Raw experiment data

TABLE V: Unstructured DeepLIFT mAP

Pruning ratio	0%	25%	50%	65%	75%	85%	90%	95%	99%
run 1	0.410	0.380	0.353	0.358	0.293	0.249	0.176	0.103	0.046
run 2	0.411	0.379	0.368	0.343	0.311	0.242	0.172	0.097	0.036
run 3	0.410	0.387	0.360	0.335	0.300	0.231	0.189	0.093	0.045
run 4	0.411	0.383	0.352	0.327	0.304	0.253	0.191	0.087	0.030
run 5	0.409	0.379	0.371	0.349	0.312	0.241	0.183	0.083	0.039
run 6	0.410	0.396	0.350	0.339	0.281	0.222	0.194	0.074	0.017
run 7	0.412	0.400	0.354	0.352	0.297	0.252	0.183	0.063	0.064
run 8	0.410	0.394	0.367	0.329	0.304	0.236	0.182	0.108	0.027
run 9	0.411	0.388	0.362	0.338	0.324	0.233	0.171	0.061	0.032
run 10	0.410	0.383	0.359	0.309	0.320	0.255	0.207	0.132	0.037
max	0.412	0.400	0.371	0.358	0.324	0.255	0.207	0.132	0.064
min	0.409	0.379	0.350	0.309	0.281	0.222	0.171	0.061	0.017
avg	0.410	0.386	0.359	0.337	0.304	0.241	0.184	0.090	0.037
std dev	8.0e-04	7.1e-03	6.9e-03	1.3e-02	1.2e-02	1.0e-02	1.0e-02	2.0e-02	1.2e-02

TABLE VI: Unstructured HYDRA mAP

Pruning ratio	0%	25%	50%	65%	75%	85%	90%	95%	99%
run 1	0.411	0.379	0.342	0.334	0.279	0.187	0.175	0.101	0.062
run 2	0.407	0.366	0.328	0.310	0.266	0.218	0.192	0.114	0.055
run 3	0.410	0.382	0.323	0.327	0.258	0.235	0.190	0.122	0.047
run 4	0.409	0.390	0.335	0.300	0.256	0.197	0.150	0.120	0.029
run 5	0.411	0.379	0.356	0.313	0.267	0.214	0.158	0.098	0.052
run 6	0.408	0.382	0.342	0.290	0.237	0.228	0.157	0.096	0.041
run 7	0.407	0.380	0.328	0.294	0.275	0.220	0.172	0.136	0.030
run 8	0.409	0.374	0.360	0.317	0.274	0.182	0.188	0.099	0.016
run 9	0.413	0.391	0.355	0.307	0.274	0.195	0.161	0.110	0.073
run 10	0.407	0.387	0.351	0.314	0.266	0.221	0.156	0.091	0.063
max	0.413	0.391	0.360	0.334	0.279	0.235	0.192	0.136	0.073
min	0.407	0.366	0.323	0.290	0.237	0.182	0.150	0.091	0.016
avg	0.409	0.381	0.342	0.311	0.265	0.210	0.170	0.109	0.047
std dev	1.9e-03	7.1e-03	1.3e-02	1.3e-02	1.2e-02	1.7e-02	1.5e-02	1.3e-02	1.7e-02

Appendix B

Appendix two text goes here.

Acknowledgment

The authors would like to thank...

TABLE VII: Structured DeepLIFT mAP

Pruning ratio	0%	25%	50%	65%	75%	85%	90%	95%	99%
run 1	0.409	0.375	0.311	0.269	0.220	0.199	0.139	0.098	0.048
run 2	0.411	0.369	0.312	0.268	0.218	0.182	0.126	0.103	0.040
run 3	0.407	0.353	0.313	0.275	0.232	0.150	0.139	0.081	0.062
run 4	0.410	0.360	0.318	0.269	0.214	0.167	0.149	0.102	0.039
run 5	0.411	0.361	0.303	0.278	0.230	0.177	0.142	0.108	0.052
run 6	0.411	0.363	0.304	0.275	0.211	0.165	0.141	0.101	0.011
run 7	0.406	0.376	0.323	0.273	0.204	0.180	0.152	0.119	0.024
run 8	0.408	0.381	0.322	0.274	0.228	0.168	0.142	0.110	0.053
run 9	0.418	0.361	0.321	0.264	0.239	0.190	0.159	0.121	0.058
run 10	0.408	0.365	0.308	0.278	0.260	0.187	0.122	0.090	0.041
max	0.418	0.381	0.323	0.278	0.260	0.199	0.159	0.121	0.062
min	0.406	0.353	0.303	0.264	0.204	0.150	0.122	0.081	0.011
avg	0.410	0.366	0.314	0.272	0.226	0.176	0.141	0.103	0.043
std dev	3.2e-03	8.2e-03	6.9e-03	4.4e-03	1.5e-02	1.4e-02	1.1e-02	1.2e-02	1.5e-02

TABLE VIII: Structured HYDRA mAP

Pruning ratio	0%	25%	50%	65%	75%	85%	90%	95%	99%
run 1	0.413	0.352	0.271	0.264	0.204	0.163	0.120	0.102	0.054
run 2	0.410	0.364	0.309	0.223	0.194	0.160	0.115	0.079	0.058
run 3	0.413	0.367	0.291	0.239	0.195	0.155	0.147	0.081	0.065
run 4	0.411	0.348	0.297	0.243	0.186	0.168	0.142	0.087	0.057
run 5	0.411	0.349	0.280	0.260	0.188	0.160	0.129	0.091	0.061
run 6	0.415	0.368	0.282	0.238	0.225	0.172	0.143	0.085	0.053
run 7	0.420	0.339	0.287	0.246	0.191	0.176	0.129	0.084	0.036
run 8	0.413	0.370	0.300	0.255	0.209	0.147	0.137	0.079	0.040
run 9	0.416	0.359	0.285	0.232	0.199	0.164	0.102	0.105	0.059
run 10	0.415	0.351	0.282	0.258	0.207	0.148	0.143	0.097	0.062
max	0.420	0.370	0.309	0.264	0.225	0.176	0.147	0.105	0.065
min	0.410	0.339	0.271	0.223	0.186	0.147	0.102	0.079	0.036
avg	0.414	0.357	0.288	0.246	0.200	0.161	0.131	0.089	0.054
std dev	2.8e-03	9.9e-03	1.1e-02	1.3e-02	1.1e-02	9.0e-03	1.4e-02	9.0e-03	9.0e-03

TABLE IX: Unstructured DeepLIFT Greyscale mAP

Pruning ratio	0%	25%	50%	65%	75%	85%	90%	95%	99%
run 1	0.329	0.312	0.281	0.236	0.201	0.194	0.175	0.087	0.034
run 2	0.328	0.318	0.287	0.247	0.192	0.158	0.127	0.096	0.049
run 3	0.331	0.321	0.272	0.228	0.218	0.161	0.138	0.110	0.050
run 4	0.326	0.317	0.256	0.254	0.225	0.157	0.131	0.101	0.026
run 5	0.331	0.313	0.267	0.233	0.218	0.181	0.180	0.105	0.044
run 6	0.337	0.326	0.283	0.264	0.205	0.186	0.133	0.106	0.055
run 7	0.330	0.319	0.265	0.224	0.224	0.184	0.155	0.111	0.038
run 8	0.334	0.312	0.290	0.248	0.197	0.183	0.140	0.141	0.046
run 9	0.330	0.316	0.284	0.262	0.214	0.169	0.133	0.116	0.042
run 10	0.335	0.312	0.268	0.235	0.225	0.167	0.127	0.081	0.024
max	0.337	0.326	0.290	0.264	0.225	0.194	0.180	0.141	0.055
min	0.326	0.312	0.256	0.224	0.192	0.157	0.127	0.081	0.024
avg	0.331	0.317	0.275	0.243	0.212	0.174	0.144	0.105	0.041
std dev	3.2e-03	4.4e-03	1.1e-02	1.3e-02	1.2e-02	1.2e-02	1.8e-02	1.6e-02	9.7e-03

TABLE X: Unstructured DeepLIFT Time

Pruning ratio	0%	25%	50%	65%	75%	85%	90%	95%	99%
run 1	118.8	113.6	98.4	87.6	73.3	55.9	49.5	44.8	45.4
run 2	119.4	113.6	100.2	88.3	73.7	55.8	49.0	44.7	41.4
run 3	119.1	113.3	99.2	87.4	74.5	56.9	50.7	45.0	39.3
run 4	118.9	113.3	98.2	89.8	75.2	57.1	49.7	44.6	42.9
run 5	118.7	113.4	100.2	87.1	73.8	57.3	51.7	44.4	46.8
run 6	118.7	113.3	99.8	87.0	75.2	56.5	50.4	44.6	43.3
run 7	119.2	114.3	97.8	87.3	74.7	58.6	51.8	45.9	44.5
run 8	119.1	113.1	99.0	88.3	73.7	58.4	50.9	46.6	43.2
run 9	119.1	113.3	99.5	88.3	75.0	57.4	51.7	43.3	41.3
run 10	118.8	113.6	97.8	86.1	72.9	58.4	48.5	46.0	44.3
max	119.4	114.3	100.2	89.8	75.2	58.6	51.8	46.6	46.8
min	118.7	113.1	97.8	86.1	72.9	55.8	48.5	43.3	39.3
avg	119.0	113.5	99.0	87.7	74.2	57.2	50.4	45.0	43.2
std dev	2.2e-01	3.2e-01	8.8e-01	9.6e-01	7.8e-01	9.6e-01	1.1e+00	9.0e-01	2.1e+00

TABLE XI: Unstructured HYDRA Time

Pruning ratio	0%	25%	50%	65%	75%	85%	90%	95%	99%
run 1	119.5	113.1	100.8	88.1	75.0	59.8	50.0	45.7	44.1
run 2	119.4	113.7	99.9	87.2	75.4	59.2	52.1	44.4	44.9
run 3	119.4	113.1	99.8	88.1	74.4	57.7	52.5	44.4	41.9
run 4	119.3	113.8	100.1	88.4	75.0	59.1	53.1	45.8	43.9
run 5	119.5	112.8	100.2	88.8	73.1	56.9	52.2	44.4	42.0
run 6	119.4	112.9	101.2	88.2	73.4	57.3	51.9	44.3	42.2
run 7	119.4	112.9	100.3	88.7	74.8	57.9	51.8	43.0	42.0
run 8	119.5	113.4	101.1	88.6	73.7	55.9	51.9	43.0	42.3
run 9	119.5	113.2	98.5	90.0	76.9	58.4	52.2	43.4	42.3
run 10	119.5	112.1	99.8	87.3	74.1	59.9	51.1	45.6	43.4
max	119.5	113.8	101.2	90.0	76.9	59.9	53.1	45.8	44.9
min	119.3	112.1	98.5	87.2	73.1	55.9	50.0	43.0	41.9
avg	119.4	113.1	100.2	88.3	74.6	58.2	51.9	44.4	42.9
std dev	6.6e-02	4.6e-01	7.4e-01	7.5e-01	1.1e+00	1.2e+00	7.9e-01	1.0e+00	1.0e+00

TABLE XII: Structured DeepLIFT Time

Pruning ratio	0%	25%	50%	65%	75%	85%	90%	95%	99%
run 1	119.4	108.2	81.2	54.4	35.1	26.7	24.9	24.1	20.1
run 2	119.3	108.0	80.9	53.0	37.1	28.0	25.5	20.4	20.5
run 3	119.3	107.9	81.3	52.3	38.0	29.2	24.5	25.9	23.9
run 4	119.2	108.1	81.9	53.1	37.2	30.0	24.1	27.6	19.7
run 5	119.7	107.4	80.1	52.1	36.6	26.2	25.6	25.3	23.2
run 6	119.3	107.8	81.7	52.2	37.4	28.3	24.6	23.4	24.7
run 7	119.3	108.1	81.4	52.7	37.5	27.6	24.9	23.6	24.7
run 8	119.4	107.8	81.1	53.0	36.4	27.9	25.0	21.4	22.9
run 9	119.5	107.4	81.8	54.4	37.0	27.7	27.8	23.0	21.2
run 10	119.6	108.1	81.8	52.1	37.6	28.5	25.3	25.0	19.2
max	119.7	108.2	81.9	54.4	38.0	30.0	27.8	27.6	24.7
min	119.2	107.4	80.1	52.1	35.1	26.2	24.1	20.4	19.2
avg	119.4	107.9	81.3	52.9	37.0	28.0	25.2	24.0	22.0
std dev	1.5e-01	2.7e-01	5.2e-01	8.2e-01	7.7e-01	1.0e+00	9.6e-01	2.0e+00	2.0e+00

TABLE XIII: Structured HYDRA Time

Pruning ratio	0%	25%	50%	65%	75%	85%	90%	95%	99%
run 1	119.5	107.2	84.3	53.9	39.1	28.3	23.8	24.1	23.2
run 2	119.7	106.4	83.1	54.7	37.9	30.1	27.0	23.7	23.9
run 3	119.3	106.5	83.0	53.7	37.0	27.3	26.1	23.0	22.8
run 4	119.4	107.2	82.9	53.0	37.9	29.9	27.0	24.2	21.8
run 5	119.3	106.6	82.6	53.5	37.4	29.9	26.0	25.0	23.6
run 6	119.2	106.2	83.0	54.2	37.6	29.5	24.5	22.9	24.7
run 7	119.6	107.4	82.9	54.9	38.7	28.3	28.3	25.3	23.4
run 8	119.3	106.9	82.5	53.9	37.1	28.9	25.2	24.7	21.6
run 9	119.7	106.8	82.2	55.2	36.9	27.6	26.0	25.1	21.8
run 10	119.5	107.0	83.3	52.6	37.8	29.7	25.2	24.2	22.8
max	119.7	107.4	84.3	55.2	39.1	30.1	28.3	25.3	24.7
min	119.2	106.2	82.2	52.6	36.9	27.3	23.8	22.9	21.6
avg	119.5	106.8	83.0	54.0	37.7	28.9	25.9	24.2	23.0
std dev	1.7e-01	3.7e-01	5.3e-01	7.8e-01	6.8e-01	9.7e-01	1.2e+00	7.9e-01	9.6e-01

TABLE XIV: Unstructured DeepLIFT Greyscale Time

Pruning ratio	0%	25%	50%	65%	75%	85%	90%	95%	99%
run 1	117.8	112.5	95.8	86.0	73.6	57.8	50.2	42.4	44.5
run 2	118.1	112.0	97.7	86.0	74.6	56.1	48.7	45.1	46.5
run 3	117.9	112.1	97.0	86.6	73.8	55.0	51.1	42.3	42.2
run 4	118.1	111.4	96.4	86.1	72.8	57.9	51.7	45.2	44.6
run 5	117.8	111.8	96.8	85.8	73.4	56.4	48.8	42.1	41.6
run 6	118.2	112.4	97.3	86.4	73.5	57.2	50.6	42.8	42.5
run 7	118.1	112.5	96.0	86.5	73.7	56.8	49.6	45.4	36.6
run 8	118.3	111.5	96.9	87.0	73.6	58.1	49.9	43.9	40.9
run 9	118.1	112.2	97.8	86.4	73.4	57.3	49.8	44.7	41.2
run 10	118.1	112.6	96.9	85.6	75.2	57.1	46.9	44.6	43.9
max	118.3	112.6	97.8	87.0	75.2	58.1	51.7	45.4	46.5
min	117.8	111.4	95.8	85.6	72.8	55.0	46.9	42.1	36.6
avg	118.0	112.1	96.9	86.2	73.8	57.0	49.7	43.9	42.4
std dev	1.6e-01	4.0e-01	6.2e-01	4.0e-01	6.4e-01	8.9e-01	1.3e+00	1.3e+00	2.6e+00

References

[1] Z. Zou, K. Chen, Z. Shi, Y. Guo, and J. Ye, *Object detection in 20 years: A survey*, 2023. arXiv: 1905.05055 [cs.CV].

[2] H. Zhang and J. Wang, *Towards adversarially robust object detection*, 2019. arXiv: 1907.10310 [cs.CV].

[3] H. Li, G. Li, and Y. Yu, *Rosa: Robust salient object detection against adversarial attacks*, 2019. arXiv: 1905.03434 [cs.CV].

[4] J. C. Costa, T. Roxo, H. Proença, and P. R. M. Inácio, *How deep learning sees the world: A survey on adversarial attacks & defenses*, 2023. arXiv: 2305.10862 [cs.CV].

[5] T. Bai, J. Luo, J. Zhao, B. Wen, and Q. Wang, *Recent advances in adversarial training for adversarial robustness*, 2021. arXiv: 2102.01356 [cs.LG].

[6] G. K. Erabati, N. Gonçalves, and H. Araujo, "Object detection in traffic scenarios - a comparison of traditional and deep learning approaches," Jul. 2020, pp. 225–237. DOI: 10.5121/csit.2020.100918.

[7] B. R. Solunke and S. R. Gengaje, "A review on traditional and deep learning based object detection methods," in *2023 International Conference on Emerging Smart Computing and Informatics (ESCI)*, 2023, pp. 1–7. DOI: 10.1109/ESCI56872.2023.10099639.

[8] S. S. A. Zaidi, M. S. Ansari, A. Aslam, N. Kanwal, M. Asghar, and B. Lee, *A survey of modern deep learning based object detection models*, 2021. arXiv: 2104.11892 [cs.CV].

[9] T.-Y. Lin *et al.*, *Microsoft coco: Common objects in context*, 2015. arXiv: 1405.0312 `[cs.CV]`.